Available online at www.sciencedirect.com
ScienceDirect
Journal of Power Sources 175 (2008) 206–210
JOURNAL OF POWER SOURCES
www.elsevier.com/locate/jpowsour

Short communication

Nanocomposite Ag–LSM solid oxide fuel cell electrodes

Tal Z. Sholklapper [a,c,*], Velimir Radmilovic [b], Craig P. Jacobson [a], Steven J. Visco [a], Lutgard C. De Jonghe [a,c]

[a] *Materials Science Division, Lawrence Berkeley National Laboratory, University of California, Berkeley, CA 94720, USA*
[b] *National Center for Electron Microscopy, Lawrence Berkeley National Laboratory, Berkeley, CA 94720, USA*
[c] *Department of Materials Science and Engineering, University of California at Berkeley, Berkeley, CA 94720, USA*

Received 11 August 2007; received in revised form 17 September 2007; accepted 17 September 2007
Available online 29 September 2007

Abstract

Advances in infiltration technology have enabled the creation of innovative electrode architectures that are key to highly effective SOFC anodes and cathodes. In this work, an Ag-infiltrated electrode has been created using a pre-sintered porous scandia-stabilized zirconia (SSZ) electrode backbone. The well-sintered SSZ provides a highly connected ion-conducting pathway throughout the electrode, while the nanometer thickness of the Ag particle layer minimizes the oxygen transport resistance that otherwise limits reaction rates in typical Ag composite electrodes. The new Ag composite electrode had minimal activation polarization by 750 °C.

The infiltration technology has allowed for incorporation of additional nanoscale electrocatalysts. Here, an Ag–LSM (strontium-doped lanthanum manganate) composite was produced, that takes advantage of each component catalyst and demonstrates a further enhanced effectiveness of the cathode Ag metal catalyst, producing relatively stable cell power densities of 316 mW cm^{-2} at 0.7 V (and 467 mW cm^{-2} peak power at ∼0.4 V) for over 500 h.

Published by Elsevier B.V.

Keywords: SOFC; Nanoparticulate; Electrodes; Silver

1. Introduction

An important evolution in SOFC development has been the aim to lower operating temperatures (*i.e.* 600–800 °C) where conventional metal alloy components may serve in the stack [1,2]. However, the usual cathode material, LSM (strontium-doped lanthanum manganate), rapidly loses its effectiveness as an electrocatalyst below 800 °C [3]. Ag has been studied as a candidate electrode material in this temperature range because of its high-catalytic activity and substantial oxygen solubility and mobility [4,5]. Initially, Ag was not pursued for SOFC's due to its volatility at high temperature (*e.g.* ∼1.3 × 10^{-5} kPa at 800 °C) [5]. In the early 1990s interest in Ag electrodes again increased when Barnett et al. suggested and later demonstrated that capping layers could largely suppress the evaporation of Ag [6–9].

To take advantage of the triple phase boundary extension seen in composite electrodes, Ag–YSZ cermets were presented [10,11]. It has been found within these cermets, that the length of the oxygen diffusion paths through the Ag was the limiting factor in electrodes with high-Ag content. High-cathode reactivity was achieved by maintaining short oxygen diffusion paths, preferably sub-micron. However, an essential problem with the Ag–YSZ cermets is Ag's low-melting point (961 °C), which does not allow for the elevated processing temperatures needed to bond the YSZ in a YSZ/Ag composite electrode to the YSZ electrolyte, thereby increasing the electrolyte/electrode impedance. To avoid the problems associated with the low-melting point of Ag, an infiltrated electrode design developed by the authors was used [12,13]. First, a porous SSZ electrode was sintered to the SSZ electrolyte at a sufficient temperature (1250 °C), and then the Ag was infiltrated into this porous SSZ cathode backbone. SSZ was chosen as the backbone material since LSM infiltrated into porous SSZ has been shown to be a stable electrode [13]. After a conditioning step, a high-surface area, thin (<100 nm) Ag layer formed over much of the well-sintered SSZ electrode backbone pore walls.

* Corresponding author at: Materials Science Division, Lawrence Berkeley National Laboratory, University of California, Berkeley, CA 94720, USA. Tel.: +1 510 486 5850.
E-mail address: tzsholklapper@lbl.gov (T.Z. Sholklapper).

0378-7753/$ – see front matter. Published by Elsevier B.V.
doi:10.1016/j.jpowsour.2007.09.051

Nanocomposite electrocatalysts also can be infiltrated, thus taking advantage of each of the individual catalyst components. Here an Ag–LSM nanocomposite is introduced, providing the advantages of both of the individual nanosized components, while increasing the stability of the Ag morphology within the electrode.

2. Methods

NiO (J.T. Baker) and SSZ (*i.e.* $(Sc_2O_3)_{0.1}(ZrO_2)_{0.9}$; from Daiichi Kigenso Kagakukokyo) (50:50 wt%) were attritor-milled in isopropanol, using zirconia balls. Dried mixtures were ground and sieved and then uniaxially pressed and pre-fired at 1100 °C for 1 h. SSZ electrolytes were formed on the NiO–SSZ anode supports by colloidal deposition [14], and were co-sintered at 1350 °C for 4 h. A suspension of SSZ and graphite was then colloidaly deposited onto the SSZ electrolyte to prepare a thin layer consisting of SSZ and graphite, with an area of 1 cm^2. The resulting trilayer structure was sintered at 1200 °C for 4 h, during which graphite was burned out, leaving a porous, well-formed SSZ network. The electrocatalysts Ag or Ag–$La_{0.85}Sr_{0.15}MnO_3$ (Ag–LSM, 50:50 vol%) were produced in a similar manner to that described in earlier papers by the authors [12,13]. Appropriate amounts of metal salt and Triton X-100 surfactant were mixed and heated to ∼100 °C and then infiltrated using a vacuum impregnation apparatus (Epovac; Struers), followed by conversion of the precursors by heating at 800 °C for 0.5 h. Platinum-paste current collectors were placed on the electrodes, and then fired on, again at 800 °C for 0.5 h.

The single cells were sealed onto an alumina tube using Aremco-552 cement, and current–voltage characteristics were obtained, using 97% H_2 + 3% H_2O as the fuel and air as the oxidant. The cell performance was determined from 600 to 750 °C with a Solartron 1255 frequency response analyzer combined with a Solartron 1286 electrochemical interface. The impedance spectra were measured under near-open circuit conditions (OCV), using a 10 mV amplitude AC signal over a frequency range of 0.1–1 MHz. The dc current–voltage (*I–V*) performance was recorded with a potentiostat–galvanostat (Princeton Applied Research Model 371). After electrochemical characterization, the cells were fractured, followed by cross-sectioning and imaging with a dual focused ion and electron beam (FIB/SEM; FEI Strata 235M) system. SEM images were taken at an angle of 52° after cross-sectioning with the FIB.

3. Results and discussion

In typical composite SOFC electrodes the reaction takes place at the triple phase boundary (TPB) between the oxidant, electrocatalyst and electrolyte, but since Ag has significant oxygen (O) conductivity, O will diffuse through the Ag to the boundary between it and the electrolyte where the oxygen reduction reaction will then occur. Therefore, as long as the O diffusion length is short enough, the Ag–SSZ composite electrodes should be completely active. This is achieved by infiltrating Ag into a preformed SSZ backbone. Fig. 1 is a schematic image of a cross-section of an SSZ backbone, which is later, infiltrated with an idealized Ag layer. Since the SSZ backbone has been pre-sintered at sufficiently high temperatures to the electrolyte it can now provide ionic conductivity throughout the electrode. Therefore, when the electrolyte backbone is infiltrated with Ag a completely active electrode is formed.

To produce the desired Ag coating as in Fig. 1, the infiltrated electrode is first conditioned by the an applied current. FIB cross-sectioned micrographs of the as infiltrated and conditioned electrode are shown in Fig. 2. As seen in Fig. 2a, the as infiltrated electrode, which has been fired to 800 °C in air, the Ag is present in highly agglomerated form, with a particle size on the order of 1 μm, and does not provide a continuous electronic pathway through the electrode. An interesting, and highly beneficial effect occurs as a result of current conditioning. After nominal operation, the Ag has spread over the ionic conducting backbone providing the electronic path through the electrode. The origin of this effect, which appears actively to oppose coarsening, is not

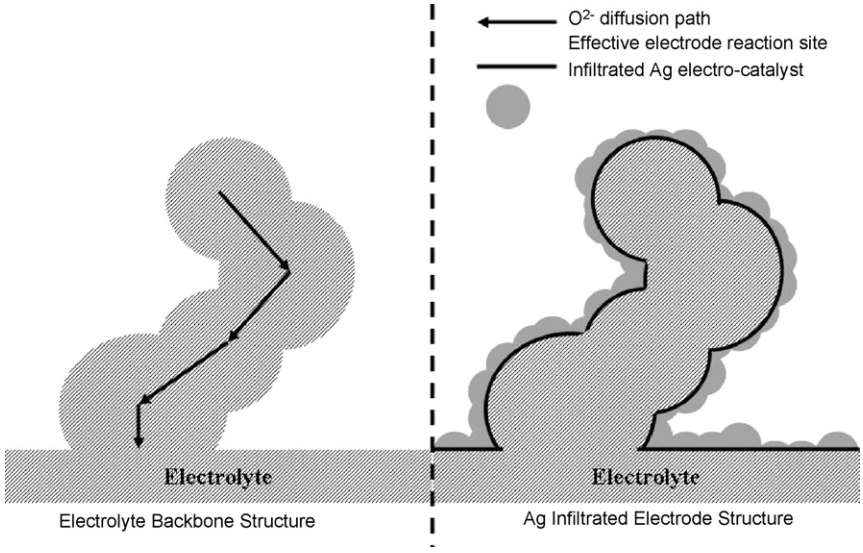

Fig. 1. Cross-sectional illustration of Ag infiltrated porous ionic conducting backbone.

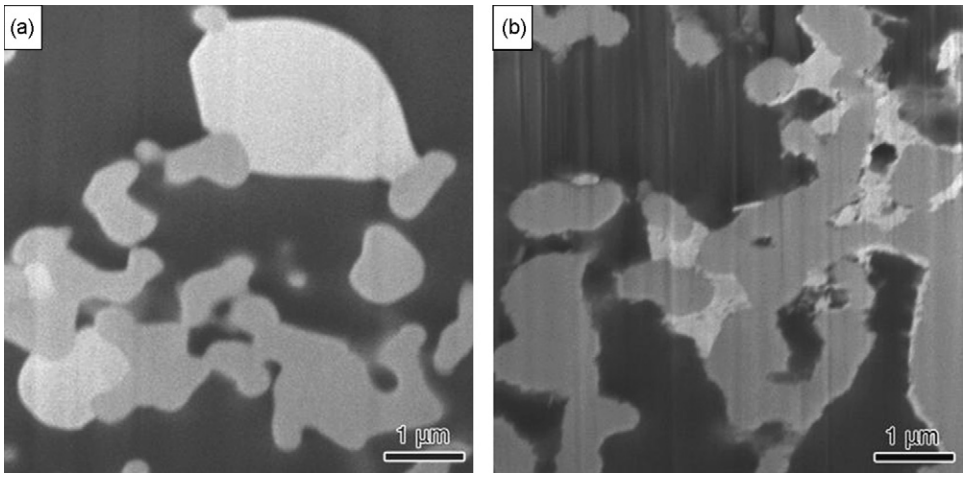

Fig. 2. SEM image of FIB cross-sectioned Ag infiltrated electrode as infiltrated (a) and after conditioning (b).

entirely understood at present, but may relate to electrochemical migration. This point is under investigation at present, in a more clearly defined geometry. It is interesting to note that measuring an IV curve was sufficient to condition the cell, as was verified by a drastic drop in cell ohmic resistance when an electronic pathway was produced through the electrode. In Fig. 2b conditioned electrode is shown after 100 h of operation. While a large fraction of the pore walls appear to be covered by Ag nanolayers ($\leq$100 nm), some pockets of micron-sized Ag remain, indicating that further microstructural improvement may be made in the electrode.

Performance curves and ac impedance spectra at 650 and 750 °C are presented in Figs. 3 and 4, respectively.

The performance curve at 650 °C shows two distinct linear activation regimes, the first between ~0.9 and 0.5 V, and the second below about 0.4 V implying that there are two processes that are inactive at OCV within this temperature range. This is also reflected in the ac impedance characteristics, where there is a large mid-frequency impedance peak found at 650 °C. The large peak at 650 °C was not previously seen in the LSM infiltrated electrodes tested by the authors [12,13]. By 750 °C the mid-frequency arc is on par with the high-frequency arc and there is only one linear activation regime, implying that the mid-frequency process was activated by 750 °C.

Previously, the authors studied LSM infiltrated electrodes [12,13] and, as is illustrated in Fig. 5a, LSM and Ag infiltrated electrodes "activate" differently, with Ag activating earlier but LSM having smaller losses after activation. The Ag electrode is activated almost right away, while the LSM electrode is only fully active by ~0.4 V. This is more clearly seen in a differential plot of $d\eta/dI$ versus $-\eta$, where the cell losses (resistance) are shown versus cell potential, Fig. 5b. By ~0.6 V, the LSM electrode has smaller losses as compared to the Ag electrode. The large post-activation losses in the Ag electrode could be due to the IR losses associated with the O transport within the silver, adding in essence an extra non-polarization activated term to the overall cell losses. It is interesting to note that the Ag–LSM nanocomposite electrode has smaller cell impedance than either of its component electrocatalysts, Fig. 6. The minimum impedance could be associated with the unique microstructure of the nanoscale electrode, Fig. 7. With the nanoscale LSM grains serving to separate nanoscale pockets of Ag (both 20–120 nm), minimizing the O diffusion length within the Ag and hence maximizing its effectiveness.

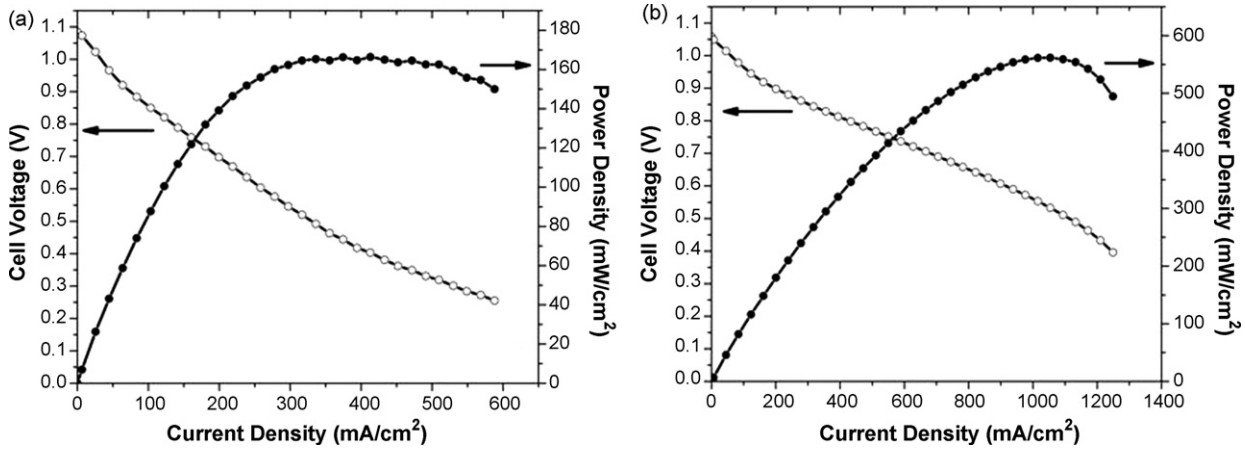

Fig. 3. Potential and power density vs. current density for an Ag infiltrated electrode at 650 °C (a) and 750 °C (b).

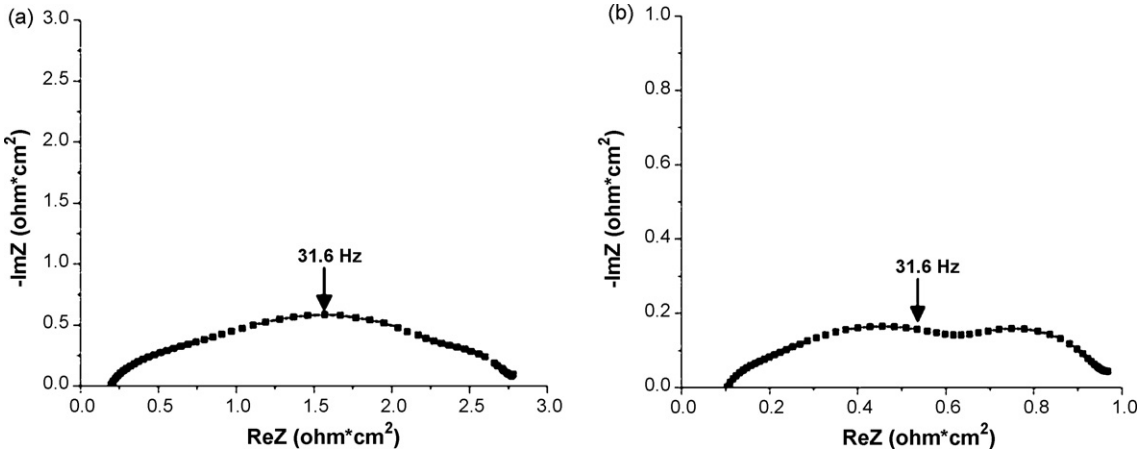

Fig. 4. Impedance spectrum for an Ag infiltrated electrode at 650 °C (a) and 750 °C (b).

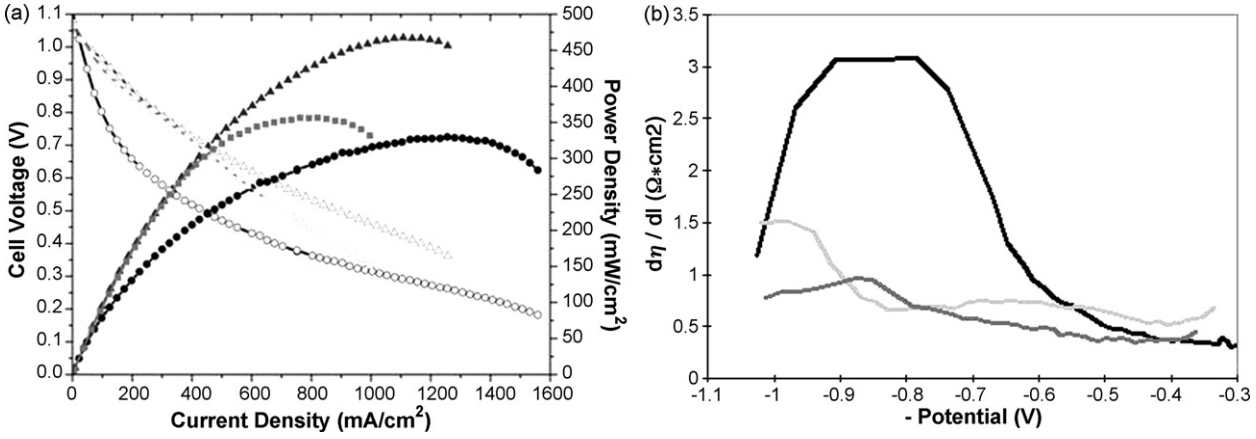

Fig. 5. Potential and power density vs. current density (a) and dη/dI vs. potential (b), for Ag (■), LSM (●) and Ag–LSM (▲) infiltrated electrodes at 700 °C.

Furthermore, the unique microstructure of the nanocomposite electrode enhanced the stability of Ag. In Fig. 8 long-term tests of Ag, LSM and the Ag–LSM nanocomposite electrode are given. The Ag cathode at 400 mA cm^{-2} shows an unsteady I–V signature, followed by progressive degradation. This non-monotonic behavior could be due to the connecting/disconnecting of the Ag network within the electrode, which would significantly affect the amount of active cell area. In contrast, the LSM electrodes are relatively stable over 500 h. In the case of this test, the cell temperature dropped after 200, decreasing the cell performance, but the LSM cell is relatively stable otherwise, as expected. The Ag–LSM nanocomposite cell, operating at 500 mA cm^{-2} showed significantly enhanced

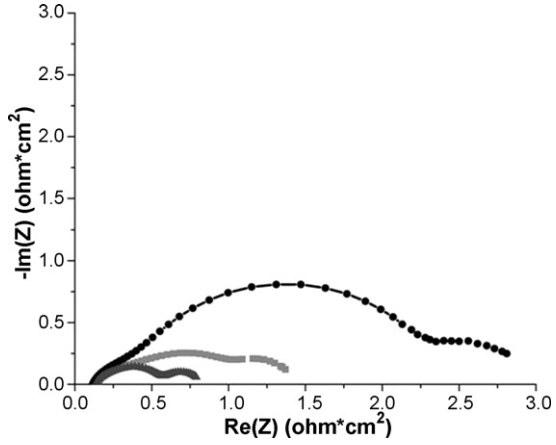

Fig. 6. Impedance spectrum for Ag (■), LSM (●) and Ag–LSM (▲) infiltrated electrodes at 700 °C.

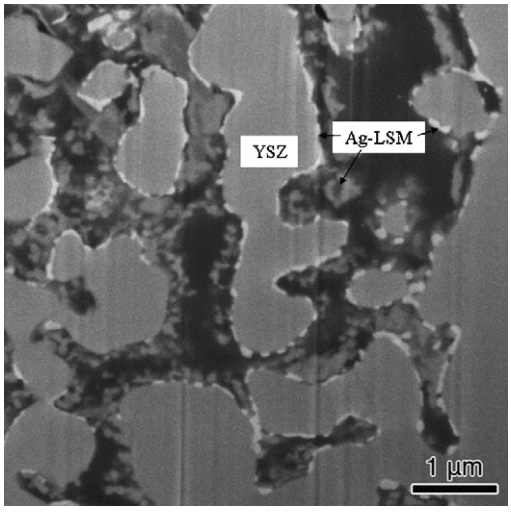

Fig. 7. SEM image of FIB cross-sectioned LSM–Ag infiltrated electrode.

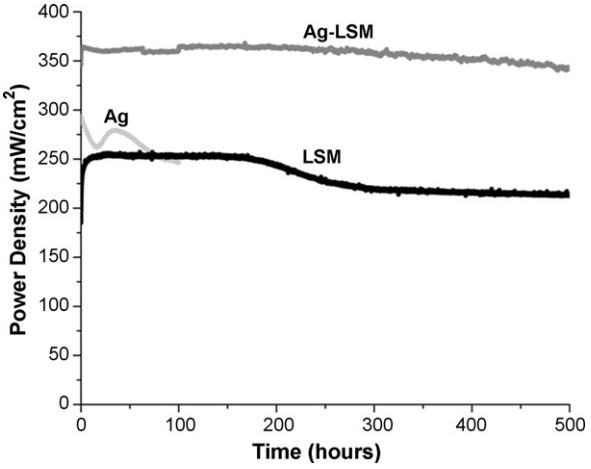

Fig. 8. Constant current operation for Ag (400 mA cm^{-2}), LSM (300 mA cm^{-2}) and Ag–LSM (500 mA cm^{-2}) infiltrated electrodes at 700 °C.

performance. It is expected that by further microstructural optimization, and perhaps the addition of a capping layer, the nanocomposite Ag–LSM can be made fully stable.

4. Conclusion

The advantages of noble metal catalysts infiltration into pre-sintered electrolyte backbones are demonstrated with Ag. Furthermore, a nanocomposite Ag–LSM cathode catalyst demonstrated the possibility of a synergistic combination of the characteristics of each of its nanocomponents. It is believed that LSM in the Ag–LSM composite may serve as a barrier to large-scale Ag agglomeration, thereby maintaining its effectiveness.

Acknowledgements

This work was supported by the U.S. Department of Energy through the National Energy Technology Laboratory. The TEM analysis was performed at the National Center for Electron Microscopy at the Lawrence Berkeley National Laboratory.

References

[1] Y. Matsuzaki, I. Yasuda, Solid State Ionics 132 (3) (2000) 271–278.
[2] M.C. Tucker, H. Kurokawa, C.P. Jacobson, L.C. De Jonghe, S.J. Visco, J. Power Sources 160 (1) (2006) 130–138.
[3] T. Tsai, S.A. Barnett, Solid State Ionics 98 (3–4) (1997) 191–196.
[4] T.L. Markin, Power Sources, vol. 4, Oriel, New York, 1973, p. 583.
[5] Tedmon Jr., et al., Cathode Materials and Performance in High-Temperature Zirconia Electrolyte Fuel Cells, J. Electrochem. Soc.: Electrochecmical Science (1969) 1170–1175.
[6] S.A. Barnett, Energy (Oxford) 15 (1) (1990) 1.
[7] L.S. Wang, E.S. Thiele, S.A. Barnett, Solid State Ionics 52 (1–3) (1992) 261.
[8] L.S. Wang, S.A. Barnett, Solid State Ionics 61 (4) (1993) 273.
[9] L.S. Wang, S.A. Barnett, Solid State Ionics 76 (1–2) (1995) 103.
[10] K. Sasaki, K. Hosoda, T.N. Lan, K. Yasumoto, S. Wang, M. Dokiya, Solid State Ionics 174 (1–4) (2004) 97.
[11] K. Sasaki, J. Tamura, M. Dokiya, Solid State Ionics 144 (3–4) (2001) 233.
[12] T.Z. Sholklapper, C. Lu, C.P. Jacobson, S.J. Visco, L.C. De Jonghe, Electrochem. Solid State Lett. 9 (8) (2006) 376–378.
[13] T.Z. Sholklapper, V. Radmilovic, C.P. Jacobson, S.J. Visco, L.C. De Jonghe, Electrochem. Solid State Lett. 10 (4) (2007) 74–76.
[14] S.J. Visco, L.-S. Wang, S. Souza, L.C. De Jonghe, Thin-film electrolytes for reduced temperature solid oxide fuel cells, Materials Research Society, Pittsburgh, PA, USA, 1995, pp. 683–695.